MFIT 1.0.0: Multiflow inversion of tracer breakthrough curves in fractured and karst aquifers

Jacques Bodin[1]

[1]Université de Poitiers, CNRS, UMR 7285 IC2MP, 40 Avenue du Recteur Pineau, 86022 Poitiers Cedex, France

5   *Correspondence to*: Jacques Bodin (jacques.bodin@univ-poitiers.fr)

Abstract. More than half of the Earth's population depends largely or entirely on fractured or karst aquifers for their drinking water supply. Both the characterization and modeling of these groundwater reservoirs are therefore of worldwide concern. Artificial tracer testing is a widely used method for the characterization of solute (including contaminant) transport in groundwater. Tracer experiments consist of a two-step procedure: 1) introducing a conservative tracer-labeled solution into an
10   aquifer, usually through a sinkhole or a well, and 2) measuring the concentration breakthrough curve (BTC) response(s) at one or several downstream monitoring locations, usually spring(s) or pumping well(s). However, the modeling and interpretation of tracer test responses can be a challenging task in some cases, notably when the BTCs exhibit multiple local peaks and/or extensive backward tailing. MFIT is a new open-source, Windows-based computer package for the analytical modeling of tracer BTCs. This software integrates four transport models that are all capable of simulating single- or multiple-peak and/or
15   heavy-tailed BTCs. The four transport models are encapsulated in a general multiflow modeling framework, which assumes that the spatial heterogeneity of an aquifer can be approximated by a combination of independent one-dimensional channels. Two of the MFIT transport models are believed to be new, as they combine the multiflow approach and the double-porosity concept, which is applied at the scale of the individual channels. Another salient feature of MFIT is its compatibility and interface with the advanced optimization tools of the PEST suite of programs. Hence, MFIT is the first BTC fitting tool that
20   allows regularized inversion and nonlinear analysis of the postcalibration uncertainty of model parameters.

1 Introduction

Artificial tracer testing is one of the most valuable methods for the characterization of flow and solute transport in groundwater. Tracer experiments consist of a two-step procedure: 1) introducing a known mass of a tracer species into an aquifer, usually through a sinkhole or well, and 2) measuring the concentration breakthrough curve (BTC) response(s) at one or several
25   downstream monitoring locations, usually spring(s) or pumping well(s). The analysis of a tracer BTC is best done by fitting a model-computed time-concentration curve to the measured values. Although spatially distributed numerical models (e.g., MODFLOW/MT3DMS or FEFLOW) can be used for this purpose, simpler (i.e., spatially lumped) models are generally used, at least in the early stages of tracer studies, either because of time constraints or because of a lack of model input data. A number of computer codes for BTC fitting have been developed in recent decades: CATTI (Sauty et al., 1992), TRACI (Käss,

30   1998, 2004), OTIS (Runkel, 1998), STANMOD (van Genuchten et al., 2012), TRAC (Gutierrez et al., 2013), OM-MADE (Tinet et al., 2019), and OptSFDM (Gharasoo et al., 2019). Note that STANMOD integrates a number of former codes, including the widely used CXTFIT code developed by Parker and van Genuchten (1984) and Toride et al. (1999). Despite the range of possibilities offered by these programs, the fitting and interpretation of tracer BTCs remains a challenging task in some cases, notably for BTCs exhibiting multiple local peaks and extensive backward tailing. Such BTC shapes, which fall in

35   the general category of non-Fickian (or anomalous) transport (Berkowitz et al., 2006; Neuman and Tartakovsky, 2009), are frequently observed in fractured and karst aquifers (Tsang and Neretnieks, 1998; Streetly et al., 2002; Massei et al., 2006; Loefgren et al., 2007; Goldscheider et al., 2008; Field and Leij, 2012; Bertrand et al., 2015; Yang et al., 2019).

To the best of the author's knowledge, only the TRACI and OM-MADE programs are able to simulate multimodal BTCs. Unfortunately, these two programs suffer from some limitations both in terms of ease of use and with respect to their

40   modeling/calibration capabilities. For instance, the TRACI software has not been maintained since 2004 and can only be used on physical or virtual computers running Windows operating system versions from Windows 98 to Windows 7. Another drawback of TRACI is the inability of the inversion (automated calibration) algorithm included in the software to handle multimodal BTCs. Each local concentration peak must be sequentially fitted through a manual (trial-and-error) calibration procedure. The OM-MADE program was written as a Python script and has neither a graphical user interface (GUI) nor inverse

45   modeling functionality. The purpose of this paper is to present a new open-source GUI-based software, named MFIT, that aims to help in the interpretation of single- or multiple-peak and/or heavy-tailed BTCs. MFIT stands for "Multi-Flow Inversion of Tracer breakthrough curves". The MFIT software integrates four transport models that can be tested against field and laboratory tracer BTCs with the assistance of the PEST automated calibration and uncertainty analysis routines (Doherty, 2019a). In its current version, the scope of the software is limited to tracer tests involving nonreactive tracer species and

50   performed in steady flow conditions. These assumptions are maintained throughout the paper.

The remainder of this paper is organized as follows. Section 2 discusses the possible origins of multiple peaks and long tails in tracer BTCs and presents the conceptual and mathematical framework of the transport models integrated in MFIT. The code implementation and coupling with PEST for automated BTC fitting are discussed in section 3. In section 4, the accuracy of MFIT-computed BTCs is verified against CXTFIT and TRACI simulations for five test cases. In section 5, we illustrate the

55   use of the software by analyzing tracer BTCs obtained in the karst aquifer of the Hydrogeological Experimental Site (HES) in Poitiers, France. The summary and conclusions are presented in section 6.

2 Multimodal and heavy-tailed BTCs: causes and modeling

Under the already mentioned assumptions (nonreactive tracer, steady-state flow), multimodal BTCs unequivocally indicate that a number of tracer-plume splittings occurred somewhere between the injection site and the monitoring point. Although

60   injection artifacts may be involved in some cases, see, e.g., Guvanasen and Guvanasen (1987), tracer splitting most commonly originates from the spreading (transverse dispersion) of the solute into areas of contrasting flow velocities; see, e.g., Moreno

Geoscientific
Model Development
Discussions

and Tsang (1991), Siirila-Woodburn et al. (2015), and Boon et al. (2017). More precisely, assuming a single-pulse tracer injection signal, multimodal BTCs reflect a three-step process: 1) tracer spreading into different flowing or nonflowing aquifer subdomains characterized by different transit/residence times, 2) tracer motion within each subdomain with little or no
65   exchange between the different subdomains, and 3) convergence (mixing) of the subtracer fluxes somewhere upstream from, or at, the monitoring point. The different models that have been proposed in the literature for simulating multimodal tracer BTCs share a common "multiflow" approach initially proposed by Zuber (1974) for the modeling of layered aquifers. In this approach, which is depicted in Fig. 1, the flow system is described as a juxtaposition of a number of one-dimensional (1-D) channels that are connected by a single common diverging (splitting) node at the entrance to the system and a single common
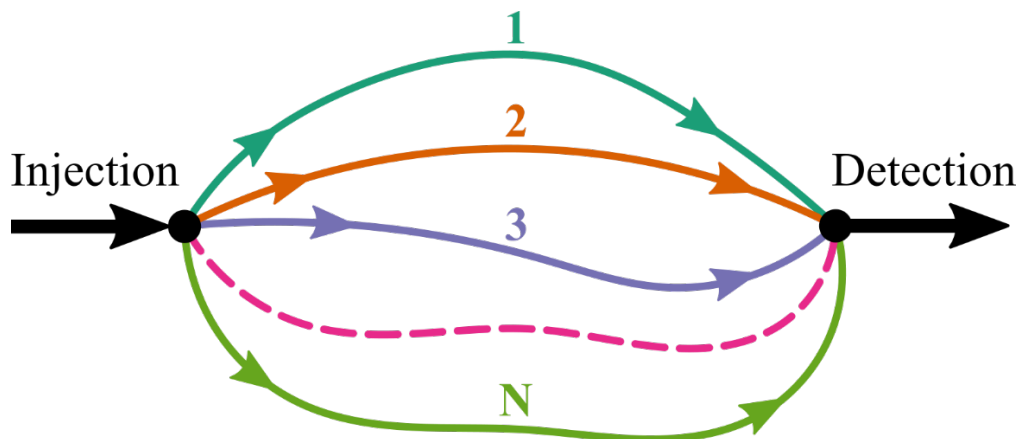70   converging (mixing) node at the outlet.

Figure 1. Conceptual sketch of the (generic) multiflow modeling approach, modified from Leibundgut et al. (2009)

In the multi-dispersion model (MDM) proposed by Maloszewski et al. (1992) and implemented in the TRACI software, the transport along each channel is assumed to obey the one-dimensional (1-D) advection-dispersion equation (ADE), and no mass
75   exchange is allowed between different channels. In the dual-advection-dispersion equation (DADE) model proposed by Field and Leij (2012), only two channels are considered. The tracer is transported by advection and dispersion along each channel, and mass exchanges between the two domains are possible. These exchanges are assumed to be governed by a first-order process. The transport model implemented in the OM-MADE code can be viewed as a generalization of the DADE model, where (i) a larger number of channels can be used, (ii) each channel can be discretized to a number of subelements with
80   different hydraulic and transport properties, and (iii) some channels can be specified as nonflowing (stagnant) water volumes. Mass exchanges between the different channels (either flowing or nonflowing) are likewise modeled as a first-order process. As pointed out above, the production of a multimodal BTC requires little or no exchange between the subtransport domains; otherwise, the mixing of the mass fluxes would rehomogenize the subtracer plumes. In accordance with this principle, small exchange coefficient values must be used in the DADE and OM-MADE models for simulating multimodal BTCs, and this
85   approach makes these models converge toward the MDM.

The interpretation of the long-tail behavior of a BTC may be more difficult than that of multiple peaks, as different mechanisms can be involved. The possible sources of extensive BTC tailing can be listed as follows: (i) tracer retention/decaying boundary condition at the injection site; (ii) tracer splitting into well-separated flow paths and then downstream convergence/mixing/overlapping of the individual pathway responses; and (iii) mass exchanges between flow domains

90   characterized by different transit/residence times. The above-listed processes are referred to below as "injection decay", "multiflow overlapping", and "multiflow exchanges", respectively. The MDM can simulate long-tailed BTCs as a result of multiflow overlapping. Multiflow exchanges are the core of the DADE model, and both multiflow overlapping and multiflow exchanges can be combined in the OM-MADE model. A number of other models have been proposed in the literature for simulating unimodal long-tailed BTCs; see, e.g., reviews in Bodin et al. (2003b), Neuman and Tartakovsky (2009), Zhang et

95   al. (2009), Dentz et al. (2011) and examples of recent works in Field and Leij (2014) and Labat and Mangin (2015). The two most commonly used models for the analysis of artificial tracer tests are the two-region nonequilibrium (2RNE) model of Toride et al. (1993), implemented in the CXTFIT code, and the single-fracture dispersion model (SFDM) of Maloszewski and Zuber (1990), implemented in TRACI and OptSFDM software. Both the 2RNE model and SFDM assume mass exchange between a single mobile (flowing) domain and a single immobile domain. A key distinction between the 2RNE model and

100   SFDM is the formulation of mass exchange, which is described as a first-order process in the 2RNE model (as in the DADE and OM-MADE models) and as a second-order (diffusion) process in the SFDM.

As already noted, multimodal and long-tailed BTCs are typical of tracer tests performed in fractured and karst aquifers. A common feature of both aquifer types is the existence of low hydraulic resistance pathways provided by the fractures and karst conduits (Tsang and Neretnieks, 1998; Worthington and Ford, 2009). A generic multiflow modeling approach is therefore

105   intuitively appealing for the interpretation of tracer tests in fractured and karst aquifers. Of course, the actual (and generally unknown) geometry of the discrete flow network experienced by the tracer is likely more complex than that depicted in Fig. 1. The channels are therefore not assumed to represent individual fractures or karst conduits but are lumped submodels of the main flow routes used by the tracer through the fractures/karst conduit network. The four transport models integrated in the MFIT software are based on the multiflow approach. The first model is a reimplementation of the MDM. The second model

110   is a variant of the MDM that assumes an exponentially decaying injection of the tracer concentration at the inlet of the flow system. In the third and fourth models, the double-porosity concept (2RNE model and SFDM) is applied at the scale of the individual channels. It is unclear whether this idea of combining multiflow and double-porosity systems is new. In the TRACI software, it is technically possible to fit a series of SFDM curves to a multimodal tracer BTC and then calculate the mean combined model curve, but to the best of the author's knowledge, this method has never been discussed or applied in the

115   literature. A possible reason is the increasing number of fitting parameters, which makes the inverse problem more complicated. The use of modern inversion tools such as PEST enables overcoming this problem, as discussed in section 3. In this article, the combination of multiflow and double-porosity systems is referred to as the multi-double porosity (MDP) approach. The immobile domain that is assigned to each flow channel is assumed to describe the porous rock matrix in contact with the fractures/karst conduits and/or any other stagnant water zones (e.g., pool volumes) adjacent to the main tracer

120 pathways. For each of the four MFIT models, the channels are assumed to be independent of each other, i.e., no mass exchange is allowed between the channels. Actually, this assumption is mathematically convenient rather than physically motivated. As already indicated, the channels are abstractions of the real main tracer pathways, which may cross (and therefore exchange between) each other between the injection site and the monitoring point. Assuming fully separated channels allows analytical modeling of mass fluxes in the multiflow system, and this approach makes the inversion of model parameters computationally

125 more efficient (see discussion in section 3).

The governing equations of the transport models are given as follows. The concentration at the outlet of a multiflow system as depicted in Fig. 1 can be calculated from the mass flux balance as follows:

$$QC = \sum_{j=1}^{N} Q_j C_j \tag{1}$$

where $Q(\text{L}^3\text{T}^{-1})$ is the total system flow rate; $C(\text{ML}^{-3})$ is the outflow concentration; N is the number of flow channels; the

130 subscript j denotes the flow channel index; and $Q_j(\text{L}^3\text{T}^{-1})$ and $C_j(\text{ML}^{-3})$ are the flow rate and concentration in the j-th channel, respectively.

The mathematical equations that have been used by Maloszewski et al. (1992) in the MDM to describe the solute transport in each flow channel are the 1-D ADE as follows:

$$\frac{\partial c_j}{\partial t} = -u_j \frac{\partial c_j}{\partial x_j} + D_j \frac{\partial^2 c_j}{\partial x_j^2} \tag{2}$$

135 and its analytical solution for the case of an instantaneous solute injection in a semi-infinite medium with both injection and detection in flux as follows (Kreft and Zuber, 1978):

$$C_j = \frac{m_j}{2Q_j T_{0j} \sqrt{\frac{\pi}{Pe_j}\left(\frac{t}{T_{0j}}\right)^3}} exp\left(-\frac{Pe_j T_{0j}}{4t}\left(1 - \frac{t}{T_{0j}}\right)^2\right) \tag{3}$$

where $t(\text{T})$ is the time variable; $x_j(\text{L})$ is the spatial coordinate along the j-th flow channel; $u_j(\text{LT}^{-1})$ and $D_j(\text{L}^2\text{T}^{-1})$ are the advection velocity and the dispersion coefficient, respectively; $m_j(\text{M})$ is the part of the solute mass flowing through the j-th

140 channel; and $T_{0j}(\text{T})$ and $Pe_j(-)$ are the mean transit time and Peclet number, respectively, as follows:

$$T_{0j} = \frac{L_j}{u_j} \tag{4}$$

$$Pe_j = \frac{u_j L_j}{D_j} \tag{5}$$

where $L_j(\text{L})$ is the length of the j-th pathway. Substituting Eq. (3) into Eq. (1) yields:

$$C = \frac{1}{Q}\sum_{j=1}^{N} \frac{m_j}{2T_{0j}\sqrt{\frac{\pi}{Pe_j}\left(\frac{t}{T_{0j}}\right)^3}} exp\left(-\frac{Pe_j T_{0j}}{4t}\left(1 - \frac{t}{T_{0j}}\right)^2\right) \tag{6}$$

145   The calibration of Eq. (6) against a tracer test BTC requires determination of the total system flow rate Q; the number N of flow channels; and for each flow channel, the values of m_j, T_{0j} and Pe_j. In this work, we generalize the above-described method by considering alternative models for the transport in individual channels and substituting the related analytical expressions of C_j into Eq. (1). The analytical transport models that are considered are (i) the solution of Eq. (2) for the case of a decaying injection boundary condition, (ii) the SFDM, and (iii) the 2RNE model.

150   The analytical solution of Eq. (2) for the case of a decaying injection boundary condition $C_j(x_j = 0, t) = C_0 \, exp(-\lambda_j t)$ was derived by Marino (1974) and can be written in the following form:

$$C_j = \frac{C_0}{2} \left[erfc\left(\left(1 + \frac{\gamma_j t}{T_{0j}}\right) \sqrt{\frac{Pe_j T_{0j}}{4t}} \right) exp\left(\frac{\gamma_j Pe_j}{2} \right) + erfc\left(\left(1 - \frac{\gamma_j t}{T_{0j}}\right) \sqrt{\frac{Pe_j T_{0j}}{4t}} \right) exp\left(\frac{-\gamma_j Pe_j}{2} \right) \right] exp\left(\frac{Pe_j}{2} \left(1 - \frac{(1-\gamma_j^2)t}{2T_{0j}} \right) \right) \quad (7)$$

where $C_0 (ML^{-3})$ is the initial (maximum) injection concentration at the inflow boundary; $\lambda_j(T^{-1})$ is the time decay constant; and

155    $\gamma_j = \sqrt{1 - \frac{4D_j \lambda_j}{u_j^2}}$ (8)

The SFDM developed by Maloszewski and Zuber (1990) describes solute transport in a double-porosity fracture-matrix system. The considered transport mechanisms are advection-dispersion in the fracture and diffusion in the surrounding rock matrix. The fracture is idealized as a parallel-plate channel, and the matrix diffusion is assumed to be unlimited, i.e., not influenced by the fluxes from other fractures. The transport equations can be written as follows:

160    $\frac{\partial C_j}{\partial t} = -u_j \frac{\partial C_j}{\partial x_j} + D_j \frac{\partial^2 C_j}{\partial x_j^2} + \frac{\theta_{pj} D_{pj}}{b_j} \frac{\partial C_{pj}}{\partial y_j}\Big|_{y_j = b_j}$ for $0 \leq y_j \leq b_j$ (9)

$\frac{\partial C_{pj}}{\partial t} = D_{pj} \frac{\partial^2 C_{pj}}{\partial y_j^2}$ for $b_j \leq y_j \leq \infty$ (10)

where $C_j(ML^{-3})$ and $C_{pj}(ML^{-3})$ are the solute concentrations in the flow channel and in the rock matrix, respectively, $\theta_{pj}(-)$ is the matrix porosity, $D_{pj}(L^2T^{-1})$ is the molecular diffusion coefficient in the matrix, $b_j(L)$ is the half-aperture of the flow channel, and $y_j(L)$ is the spatial coordinate perpendicular to the channel extension. The solution to Eqs. (9) and (10) for the case of an

165   instantaneous injection is:

$$C_j = \frac{m_j \beta_j \sqrt{Pe_j T_{0j}}}{2\pi Q_j} \int_0^t \frac{exp\left(-\frac{Pe_j(T_{0j}-\xi)^2}{4T_{0j}\xi} - \frac{\beta_j^2 \xi^2}{t-\xi} \right)}{\sqrt{\xi(t-\xi)^3}} d\xi \quad (11)$$

where $\xi(T)$ is the integration variable and $\beta_j(T^{-1/2})$ is the so-called diffusion parameter defined as:

6

$$\beta_j = \frac{\theta_{pj}\sqrt{D_{pj}}}{2b_j} \tag{12}$$

Coats and Smith (1964) proposed a different mathematical formulation of solute mass exchange between flowing and stagnant
170   water regions in double-porosity media, well known in the literature either as the mobile-immobile (MIM) model or as the
2RNE model as follows:

$$\theta_j \frac{\partial C_j}{\partial t} + \theta_{imj} \frac{\partial C_{imj}}{\partial t} = \theta_j \left(-u_j \frac{\partial C_j}{\partial x_j} + D_j \frac{\partial^2 C_j}{\partial x_j^2} \right) \tag{13}$$

$$\theta_{imj} \frac{\partial C_{imj}}{\partial t} = \alpha_j \left(C_j - C_{imj} \right) \tag{14}$$

where $\theta_j(-)$ and $\theta_{imj}(-)$ are the mobile and immobile volumetric water contents, respectively, $C_{imj}(ML^{-3})$ is the concentration
175   in the immobile domain, and $\alpha_j(T^{-1})$ is a first-order mass transfer coefficient. The two main differences with respect to the
SFDM are (i) the dual-domain formulation of the problem (mobile and immobile regions are assumed to coexist at each point
in space, and this assumption differs from the parallel-plate channel geometry in the SFDM) and that (ii) the solute mass
exchange between mobile and immobile domains is assumed to be governed by a first-order process, whereas the SFDM refers
to the second-order diffusion Eq. (10). Building on a general set of analytical solutions developed by Toride et al. (1993), the
180   solution of the 2RNE model for the case of an instantaneous injection can be written as follows:

$$C_j = \frac{m_j}{Q_j} \left[\frac{1}{T_{0j}\sqrt{\frac{4\pi}{Pe_j}\left(\frac{t}{T_{0j}}\right)^3}} exp\left(-\frac{Pe_j\left(1-\frac{t}{T_{0j}}\right)^2}{4\frac{t}{T_{0j}}} - \omega_j L_j \frac{t}{T_{0j}} \right) \right.$$
$$\left. + \frac{\omega_j \psi_j}{T_{0j}} \sqrt{\frac{L_j^3 Pe_j}{4\pi(1-\psi_j)}} \int_0^{\psi_j L_j \frac{t}{T_{0j}}} \frac{1}{\tau\sqrt{\psi_j L_j \frac{t}{T_{0j}} - \tau}} exp\left(-\frac{Pe_j(\psi_j L_j - \tau)^2}{4\psi_j L_j \tau} - \frac{\omega_j \tau}{\psi_j} - \frac{\omega_j\left(\psi_j L_j \frac{t}{T_{0j}} - \tau\right)}{1-\psi_j} \right) I_1\left(2\omega_j\sqrt{\frac{\tau\left(\psi_j L_j \frac{t}{T_{0j}} - \tau\right)}{\psi_j(1-\psi_j)}} \right) d\tau \right]$$
$$\tag{15}$$

where I_1 is the modified Bessel function of the first kind; $\tau(L)$ is the integration variable; and

$$\psi_j = \frac{\theta_j}{\theta_j + \theta_{imj}} \tag{16}$$

185    $$\omega_j = \frac{\alpha_j}{\theta_j u_j} \tag{17}$$

It is notable that when $\psi_j=1$ and $\omega_j=0$, Eq. (15) simplifies to Eq. (3). Table 1 summarizes the parameters of the four MFIT
transport models.

Table 1. Parameters of the transport models integrated in the MFIT software. The subscript j denotes a parameter that must be defined for each flow channel. The parameters without this subscript are common to all channels.

Model	Parameters	Maximum number of calibration parameters for an n-channel solution
MDMi (ADE, instantaneous injection)	Q, m_j, T_{0j}, Pe_j	$3n+1$
MDMed (ADE, exponentially decaying injection)	$C_0, Q_j/Q, T_{0j}, Pe_j, \gamma_j$	$4n+1$
MD2P-SFDM	$Q, m_j, T_{0j}, Pe_j, \beta_j$	$4n+1$
MD2P-2RNE	$Q, m_j, L_j, T_{0j}, Pe_j, \psi_j, \omega_j$	$6n+1$

3 Code implementation and inversion

The four analytical models described in the previous section have been implemented in C++ and compiled as executable Windows programs named MDMi.exe (for MDM, instantaneous injection), MDMed.exe (for MDM, exponentially decaying injection), MDP_SFDM.exe, and MDP_2RNE.exe. The code and executable files are freely available on the public Zenodo repository https://doi.org/10.5281/zenodo.3470751. In the MDP_SFDM and MDP_2RNE programs, the numerical evaluation of the integrals in Eqs. (11) and (15) is performed using the QAG adaptive integration routine from the GNU Scientific Library with a 61-point Gauss-Kronrod rule and a relative error convergence criterion of 10^{-2}. These four programs can be run as console applications to solve a direct (forward) problem, i.e., computing a series of time-concentration values for a given set of model parameters. Both the input and output files are in ASCII format and can be edited with any text editor program for pre-/postprocessing. A convenient alternative is to use the MFIT software as a GUI for these applications. The MFIT software has been developed using the C++ Builder environment (Embarcadero RAD Studio 10.1 Berlin) and provides a GUI for (i) importation and graphic visualization of user-provided BTC data; (ii) parameterization, direct running, and graphical output of the analytical transport models; (iii) inversion (automatic calibration) of model parameters for optimal curve fitting; and (iv) assessment of the uncertainty of calibrated parameter values.

Both the optimization and uncertainty analysis of model parameters are carried out using PEST routines (Doherty, 2019a, 2019b). PEST is a public domain model-independent program suite that has been widely used over the past two decades, notably in the field of surface and subsurface hydrology (e.g., Long, 2015; Woodward et al., 2016; Gaudard et al., 2017; Wang et al., 2019). The theoretical framework and full range of capabilities of the PEST software are well documented (Doherty et al., 2010; Doherty, 2015, 2019a, 2019b) and are not repeated here. Only the concepts and methods that were deemed to be the

210   most relevant to the multiflow modeling approach and that have been made accessible through the MFIT GUI software are
briefly reviewed below.

PEST is based on a gradient optimization method and, as such, requires the derivatives of model outputs with respect to the
adjustable model parameters to be calculated in each iteration for implementing the Jacobian (sensitivity) matrix. As pointed
out by Doherty (2015), the accuracy of these derivative calculations is critical to the performance of the PEST optimization

215   algorithm. In the MFIT program suite, most of the model partial derivatives are calculated analytically and externally provided
to PEST. This approach ensures both the accuracy and speed of this part of the optimization process. Less straightforward
partial derivative expressions were derived using MAPLE and exported as C code using the MAPLE code generation routine.
The partial derivative functions were implemented in the MDMi, MDMed, MDP_SFDM, and MDP_2RNE programs and are
processed during the PEST system calls to these programs by providing an optional "/d" command line argument to the

220   program name. In a few cases, however, the partial derivatives cannot be calculated analytically, as they involve undefined
limits. Such is the case for the derivatives of Eq. (15) with respect to the parameters ψ_j, L_j and T_{0j}. In these cases, the partial
derivatives are computed by PEST using finite differences.

The calibration of a multiflow transport model against a tracer BTC is hampered by two well-known issues in inverse modeling:
(i) model nonlinearity and (ii) solution nonuniqueness. Both issues may cause numerical instabilities that can prevent the

225   inversion algorithm from converging to the optimal solution. PEST includes two regularization methods that can be used either
individually or together to guide the optimization process. The singular value decomposition (SVD) method subtracts
parameter combinations for which the tracer BTC is uninformative. The inversion is conducted on the basis of a reduced set
of orthogonal linear combinations of the model parameters rather than attempting to estimate the parameters individually. The
Tikhonov regularization method provides a different but complementary strategy, where the information content of the tracer

230   BTC is supplemented with expert knowledge pertaining to the model parameters. When using Tikhonov regularization, the
objective function that is minimized by PEST is defined as the sum of two terms. The first term is the "measurement objective
function" and is defined as the sum of the squared weighted differences between the real tracer BTC and the model-simulated
curve. The second term is referred to as the "regularization objective function" and acts as a penalty function for deviations
from some preferred parameter conditions. Two Tikhonov regularization options have been implemented in MFIT. The first

235   option, referred to as "preferred homogeneity", promotes a solution of minimum variance for the model parameters pertaining
to the different channels. In the second option, referred to as "preferred value", the optimization process seeks the solution that
is the closest to some prior estimates of the model parameters.

Unfortunately, neither SVD nor Tikhonov regularization can guarantee that the PEST optimization algorithm will converge to
the global optimal solution in the parameter space. Where local minima exist in the objective function, which is the rule rather

240   than the exception with nonlinear models, the optimization process may become trapped and fail to identify existing better
solutions (Singh et al., 2012; Espinet and Shoemaker, 2013; Abdelaziz et al., 2019). A central issue in this case is the sensitivity
to initial parameter values, i.e., different initial parameter sets may lead to different optimized solutions. Global optimization
methods have been proposed in the literature to overcome this issue; see, e.g., Arsenault et al. (2014) for a review and

comparison of various algorithms. The PEST program suite includes two such global optimizers based on the SCE-UA method

245 (Duan et al., 1992) and the CMA-ES method (Hansen and Ostermeier, 2001). The corresponding programs are named SCEUA_P and CMAES_P, respectively. It must be noted, however, that global optimization methods suffer from their own drawbacks, including sensitivity to tuning parameters and low computational efficiency. An alternative strategy to improve the chances of convergence toward the global optimum with gradient-based methods is the "multistart" approach, which consists of repeating the optimization process starting from different initial parameter value sets (Skahill and Doherty, 2006;

250 Piotrowski and Napiorkowski, 2011). Such a strategy has been implemented in the MFIT software. The key principle of the proposed algorithm is that rather than conducting the optimization for a fixed number N of channels only, a series of automatic tracer BTC fittings is performed for a decreasing number of channels ranging from N_{max} to 1. The main steps of the MFIT multistart algorithm are detailed as follows:

1. The first optimization is performed by considering the maximum number of flow channels, N_{max}. The initial transport

255   parameters are automatically tuned by MFIT to obtain N_{max} well-separated concentration peaks. For this goal, the tracer BTC is first analyzed to determine the times T_5 and T_{95}, defined as follows:

$$T_5 = max(T_{5th}, 1.1 \times T_{min}) \tag{18}$$

$$T_{95} = min(T_{95th}, 0.9 \times T_{max}) \tag{19}$$

Where T_{5th} and T_{95th} are the earliest and latest times at which the concentration values are above and below 5 % of the

260   maximum concentration value, respectively, and T_{min} and T_{max} are the minimum and maximum time values of the user-provided BTC, respectively. The mean travel times T_{0j} are then uniformly distributed between the times T_5 and T_{95}. Next, the initial Peclet number Pe_j of each channel is calculated as:

$$Pe_j = \left(15 \frac{N_{max}T_{0j}}{T_{95}-T_5}\right)^2 \tag{20}$$

Equation (20) is based on a semiempirical relationship between the standard deviation of travel times for transport by

265   advection and dispersion, $\sigma_j = T_{0j}\sqrt{2/Pe_j}$ (see, e.g., Bodin et al. 2003a, Eq. 10), and the time span of the j-th concentration peak, which is on the order of $6\sigma_j$. The constraint of well-separated concentration peaks may be formulated as $6\sigma_j N_{max} << (T_{95}-T_5)$, which is verified by Eq. (20). The initial values of the other transport parameters in Eqs. (7), (11), and (15) are chosen to minimize the tailing effect due to noninstantaneous injection or solute mass exchange between flowing and stagnant water regions as follows: $\gamma_j = 0.1$, $\beta_j = 0.001$, $\psi_j = 0.9$, and $\omega_j = 0.05$.

270 2. Once the optimization has been performed for the N_{max} channel model, the next step is to optimize the transport parameters for $N_{max}-1$ channels. The multistart optimization approach begins here as not only one but N_{max} optimizations are performed in this step. The initial parameter values for the $N_{max}-1$ channels are initialized from the previously optimized N_{max} channel solution by sequentially removing one of the channels. Only the solution corresponding to the lowest sum of the squared weighted differences between the tracer BTC and model-simulated curve is retained.

275 3. This procedure is repeated up to the single-channel solution. The total number of PEST optimizations is $N_{max}(N_{max}+1)/2$.

Calling the multistart algorithm has been made optional in MFIT, as this algorithm significantly increases the computational cost and running time of the optimization process. However, experience has shown that the multistart approach can truly improve the model fit results and can be worth the effort in many circumstances. A comparison between optimizations conducted by the PEST multistart algorithm and the global SCE-UA and CMA-ES methods was conducted in this study and

280   is discussed in section 5.

Because of the nonuniqueness of the inverse problem, some uncertainties may be associated with the PEST-optimized model parameter values. A nonlinear analysis method has been implemented in MFIT for the assessment of postcalibration parameter uncertainty. The algorithm can be described by the following steps: 1) compute a linear approximation to the posterior parameter covariance matrix by using the PEST PREDUNC7 utility; 2) sample the posterior parameter covariance matrix, and

285   generate multiple calibration-constrained random parameter sets using the PEST RANDPAR utility; 3) recalibrate each parameter set with PEST up to achieving a level of fit fairly similar to the original calibration result (a tolerance of +5 % for the measurement objective function is allowed by MFIT); and 4) compute histograms of the recalibrated parameter values. The following two assumptions underlie this method: (i) the upper and lower parameter bounds specified by the user for the PEST inversion reflect the prior (expert knowledge) parameter uncertainty, and (ii) the model parameters are statistically

290   independent from a prior point of view. This second assumption is relaxed through the recalibration process.

4 Code verification

The robustness of the PEST inversion program has been demonstrated in a number of studies, see, e.g., Anderson et al. (2015) and Hunt et al. (2019), and is not reassessed here. The purpose of this section is to assess the accuracy of MFIT direct simulations through five synthetic test cases. Tests 1 and 2 address the case of a single flow channel described as a single-

295   porosity medium in which the transport is governed by advection-dispersion. An instantaneous injection of the tracer is assumed in test 1, whereas test 2 addresses the case of an exponentially decaying concentration at the inlet. A double-porosity medium, single flow channel is assumed in tests 3 and 4, which conform to the assumptions of the SFDM and 2RNE model, respectively. In test 5, the tracer is transported by advection-dispersion in a multiflow system composed of three channels. This scenario corresponds to the MDM. The input parameters for the five test cases are listed in Table 2. The BTCs simulated

300   by MFIT for tests 1, 2 and 4 are compared to those obtained by CXTFIT. The MFIT simulations for tests 3 and 5 are compared against those obtained by TRACI. As shown in Fig. 2, very good agreement was obtained in each case.

Geoscientific
Model Development
Discussions

Table 2. Input parameters for the five verification tests.

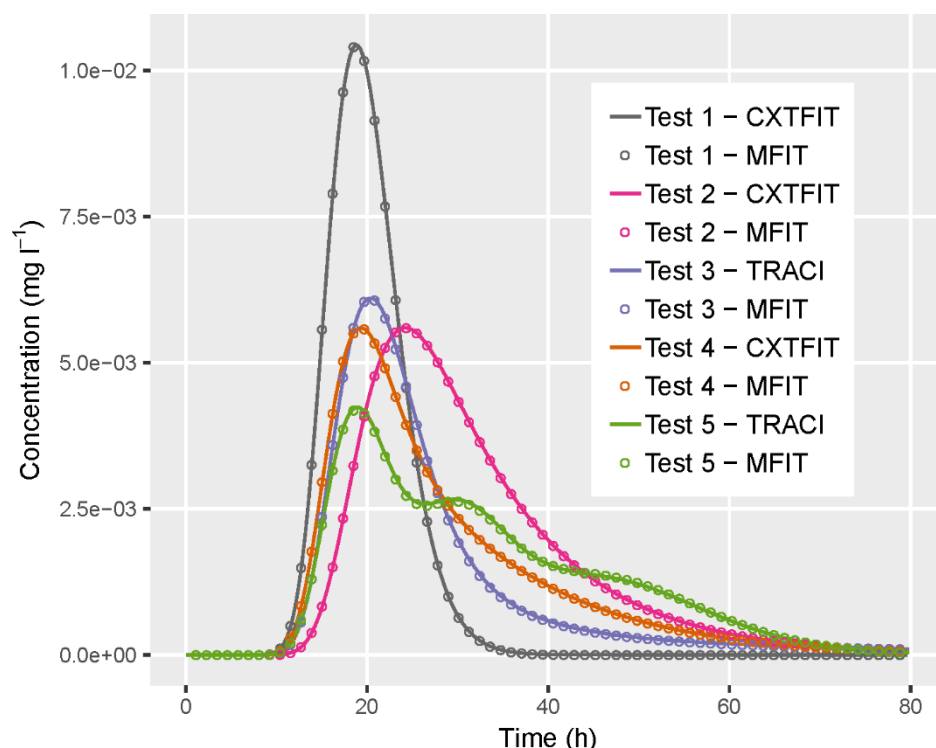| Test	Parameters	Values
1 **(single flow channel, ADE, instantaneous injection)**	Flow rate Q	10 m^3 h^{-1}
	Injected mass m	1 g
	Mean transit time T_0	20 h
	Peclet number Pe	50
2 **(single flow channel, ADE, exponentially decaying injection)**	T_0, Pe	same as Test 1
	Initial (maximum) injection concentration C_0	0.01 mg l^{-1}
	Gamma coefficient γ	0.93
3 **(single flow channel, SFDM)**	Q, m, T_0, Pe	same as Test 1
	Diffusion parameter β	0.04 h$^{-1/2}$
4 **(single flow channel, 2RNE)**	Q, m, T_0, Pe	same as Test 1
	Length of the flow channel L	10 m
	Fraction of mobile water ψ	0.7
	Omega coefficient ω	0.1 m^{-1}
5 **(three channels, MDM-ADE)**	Total system flow rate Q	10 m^3 h^{-1}
	Mass flowing through the first channel m_1	0.4 g
	Mass flowing through the second channel m_2	0.3 g
	Mass flowing through the third channel m_3	0.3 g
	Mean transit time in the first channel T_{01}	20 h
	Mean transit time in the second channel T_{02}	32 h
	Mean transit time in the third channel T_{03}	50 h
	Peclet number in the first channel Pe_1	50
	Peclet number in the second channel Pe_2	70
	Peclet number in the third channel Pe_3	50

305

Figure 2. Comparison among MFIT, CXTFIT, and TRACI simulations for test 1 (single flow channel, ADE, instantaneous injection), test 2 (single flow channel, ADE, exponentially decaying injection), test 3 (single flow channel, SFDM), test 4 (single flow channel, 2RNE), and test 5 (three channels, MDM-ADE)

5 Application example: analysis of tracer BTCs from the Hydrogeological Experimental Site in Poitiers, France

The HES is a field research facility operated by the University of Poitiers, France. The facility consists of 32 wells that have been drilled within an overall area of 0.2 km² (Fig. 3) and that fully penetrate a 100 m thick confined limestone aquifer. The interwell flow and transport connectivity have been shown to be mainly related to karst conduits, 0.01–3 m in diameter, that develop preferentially within specific lithostratigraphic horizons interbedded with nonkarstified limestone units. The karstified layers may contribute to the connectivity from one well to another either directly (e.g., the wells intersect with the same karst network in a single layer) or indirectly (e.g., the wells intersect with different karst network layers that are interconnected by either a third well or a subvertical fracture); see Audouin et al. (2008) and Chatelier et al. (2011).

13

Figure 3. The locations of wells at the HES in Poitiers, France. Map data are from © Google.

A large number of pumping test experiments have been conducted at the HES since 2002. As discussed in a number of studies (Delay et al., 2007; Riva et al., 2009; Delay et al., 2011; Bodin et al., 2012; Sanchez-Vila et al., 2016; Le Coz et al., 2017), the drawdown responses exhibit complex behaviors, which are likely due to the strong aquifer heterogeneity induced predominantly by the presence of karst features. In addition to the pumping test experiments, a number of cross-borehole tracer tests have been performed at the HES since 2011. The standard experimental protocol of HES tracer experiments can be summarized as follows:

1. Starting a pumping experiment and waiting for the establishment of a pseudosteady state flow regime (i.e., stabilization of interwell piezometric head gradients), which typically takes approximately 6 h at the HES;

2. Performing flow log measurements in the candidate injection well to identify the main inflow/outflow levels along the well bore;

14

3. Connecting a series of 2.5 m length and 1.5 cm inner diameter PVC pipes in the injection well, from the ground down to the tracer injection depth (usually chosen to be as close as possible to a main outflow level). The pipeline is terminated by a 5 cm length screened cap that ensures a horizontal outflow of the tracer solution in the injection well.

4. Injecting a tracer solution (typically 2 l of uranine solution at 1 g l^{-1}) in the pipe and flushing with 40 l of "clean" ground
335   water. The total duration of an injection is typically less than 3 min.

5. Monitoring the tracer BTC at the pumped well using a flow-through fluorometer (Albillia GGUN-FL22) connected to a branch pipe extending from the discharge line at ground level. The fluorometer is periodically calibrated in the laboratory with solutions of 10 µg l^{-1} and 100 µg l^{-1}.

To date, more than 70 cross-well tracer experiments have been performed at the HES. The purpose here is not to interpret each
340   of these experiments but to pick a few examples for illustrating the application of the MFIT software. The selected data correspond to three tracer experiments that were performed in 2016 and 2017 using well M22 as the pumped well and M16, MP6, and P2 as injection wells. Fig. 4 shows the experimental BTCs and a collection of calibrated MFIT curves for different numbers of channels. The selected experiments were chosen for their representativeness of the BTC shapes observed at the HES, which exhibit either a single peak followed by a more or less pronounced tailing, e.g., P2-M22, overlapping double-peak
345   responses, e.g., M16-M22, or well-marked multimodal responses, e.g., MP6-M22. The model fit results shown in Fig. 4 were obtained using the multistart method discussed in section 3 and only SVD as a regularization tool for the inversion. None of the model parameters were fixed, and all were optimized within realistic upper and lower limits.

Beyond what can be visually inferred from Fig. 4, the assessment of the relative fitting performance of the different models can be analyzed through the evolution of the measurement objective function, hereafter named PHI, with respect to the number
350   N of channels and/or the number P of optimized model parameters. Fig. 5 displays the PHI(N) and PHI(P) curves summarizing the best-fitting results achieved with the use of the multistart PEST optimization and with the use of the SCEUA_P and CMAES_P global optimization routines. A number of observations can be made from this figure. As a first remark, the SCEUA curves for the two MDP models are missing in Fig. 5. The reason is that the SCEUA_P program has no "forgive–error" capability, i.e., if a set of trial parameters causes the numerical evaluation of Eq. (11) or Eq. (15) to crash, the optimization
355   process is stopped instead of moving to a new set of parameter values. Such a forgiveness option is available in the PEST and CMAES_P programs. The next observations that can be made from Fig. 5 are that the CMAES and SCEUA curves are (i) more irregular, (ii) always above or equal to their PEST-computed counterparts, and (iii) do not always follow the expected decreasing trend in the PHI value (meaning a better model fit) as the number of channels rises, as depicted by the PEST curves. However, it must be mentioned that the number of optimization runs was much greater for the CMAES_P and SCEUA_P
360   programs, and various optimization options were tested (e.g., changing the upper and lower parameter bounds and log-transformation of parameters). The CMAES and SCEUA curves shown in Fig. 5 are actually the "best results" obtained after several days of computation time. It is clear that the multistart PEST optimization method performs better in each case.

The PHI curves obtained by PEST can be viewed as Pareto curves illustrating the tradeoff between the model fitting quality and the number of channels or the number of calibration parameters. It must be noted that since no Tikhonov regularization

365 was used in this illustration example, the model inversion results for higher *N* values are likely affected by overfitting. More reliable parameter values could be obtained by adding Tikhonov regularization constraints to the optimization process.
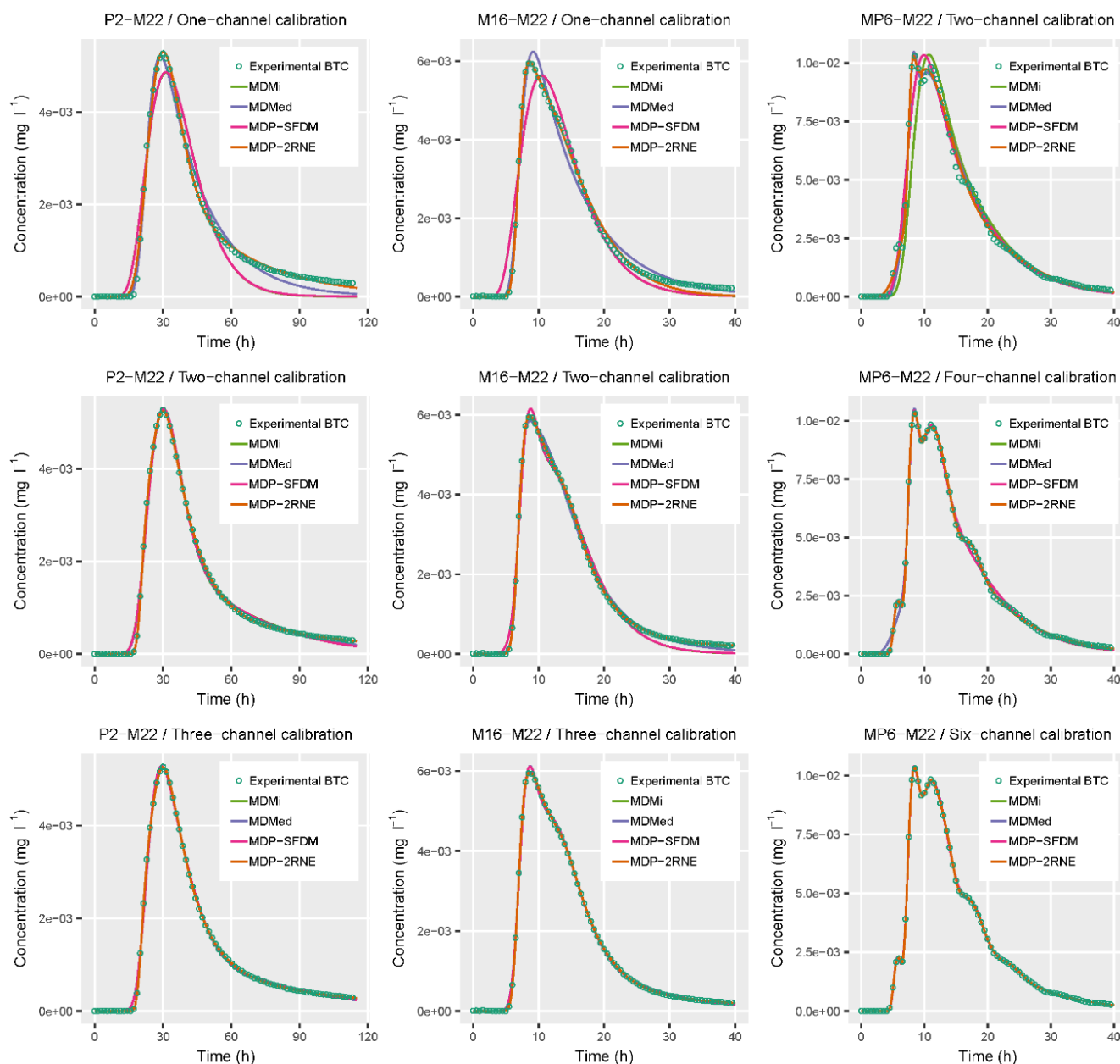

Figure 4. Inversion solutions of three tracer BTCs for different numbers of channels. Some model curves are hardly distinguishable, as they perfectly overlap (see text and Fig. 5).
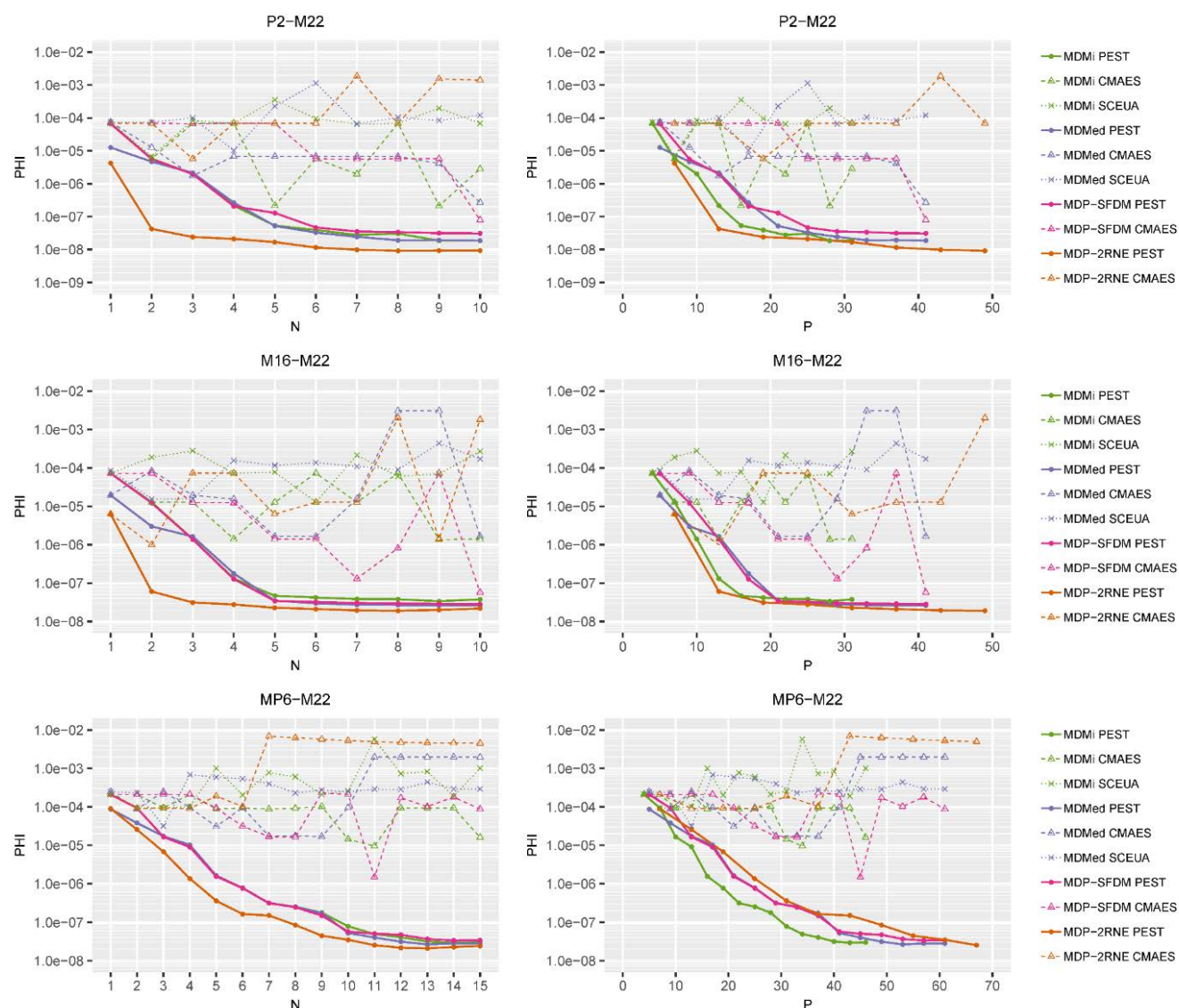
370

Figure 5. Best-fitting performance of the multiflow models achieved with the use of PEST with the multistart optimization approach and with the use of global optimizers. *N* is the number of channels in the models, *P* is the number of optimized parameters, and PHI is the sum of the squared weighted differences between the tracer BTCs and the model-fitted curves.

According to the PHI(N) curves shown in Fig. 5, the MDMi model and MDP-SFDM perform similarly for the three tracer tests, and the related PHI(N) curves are hardly differentiable. This result was expected, as the short duration of the HES tracer tests, typically from a few hours to a few days, makes the matrix diffusion process unlikely to be significant. Assuming

exponential decaying (MDMed) instead of instantaneous (MDMi) injection gives slightly better fitting results for a low number

380   of channels but provides no benefit for a moderate to high number of channels. Also according to the PHI(N) curves, the fitting

performance of the MDP-2RNE model seems significantly better than that of the three other models. However, this observation

must be counterbalanced by the larger number of calibration parameters in the MDP-2RNE model (see Table 1). A two-channel

MDP-2RNE model involves 13 parameters, which corresponds to the number of parameters in a four-channel MDMi model.

The PHI(P) curves shown in Fig. 5 provide a fairer assessment of the fitting performance of the different models. According

385   to these curves, the MDP-2RNE model performs slightly better than the MDMi model for the P2-M22 tracer test (single-peak

slightly tailed BTC), almost equally well for the M16-M22 tracer test (overlapping double peaks), and worse for the MP6-

M22 tracer test (well-marked multimodal BTC). It must be appreciated that these two models should not be opposed to each

other. Both models likely provide an equally valid description of the tracer transport in the HES aquifer while relying on

different conceptualizations of the medium heterogeneity.

390   An example of postcalibration uncertainty analysis is shown in Fig. 6, which illustrates the uncertainty of parameter values

pertaining to the inversion of the M16-M22 tracer BTC by a two-channel MDMi model. Owing to the balance between the Q

and m_j terms in Eq. (6), at least one of these parameters must be fixed for the uncertainty of the others to be assessed. Here,

the value of Q was set to 60.3 m^3 h^{-1}, which corresponds to the pumping rate in the experiment. Following the PEST

optimization of the 6 other model parameters (m_1, m_2, T_{01}, T_{02}, Pe_1, Pe_2), 500 calibration-constrained parameter fields were

395   stochastically generated and recalibrated by PEST. Of these 500 recalibration runs, 499 successfully achieved a level of fit

fairly similar to that associated with the original calibration parameter field. The histograms shown in Fig. 6 were constructed

from these 499 recalibrated parameter sets and illustrate the uncertainty in the calibrated model parameter values. As shown

in this figure, the confidence interval for each parameter is quite narrow, except for the Peclet number related to the first

channel, which has a medium uncertainty. This finding suggests that the first BTC peak is not well fitted by the two-channel

400   MDMi model and that either more channels or a different model should be taken into consideration for a more precise fitting
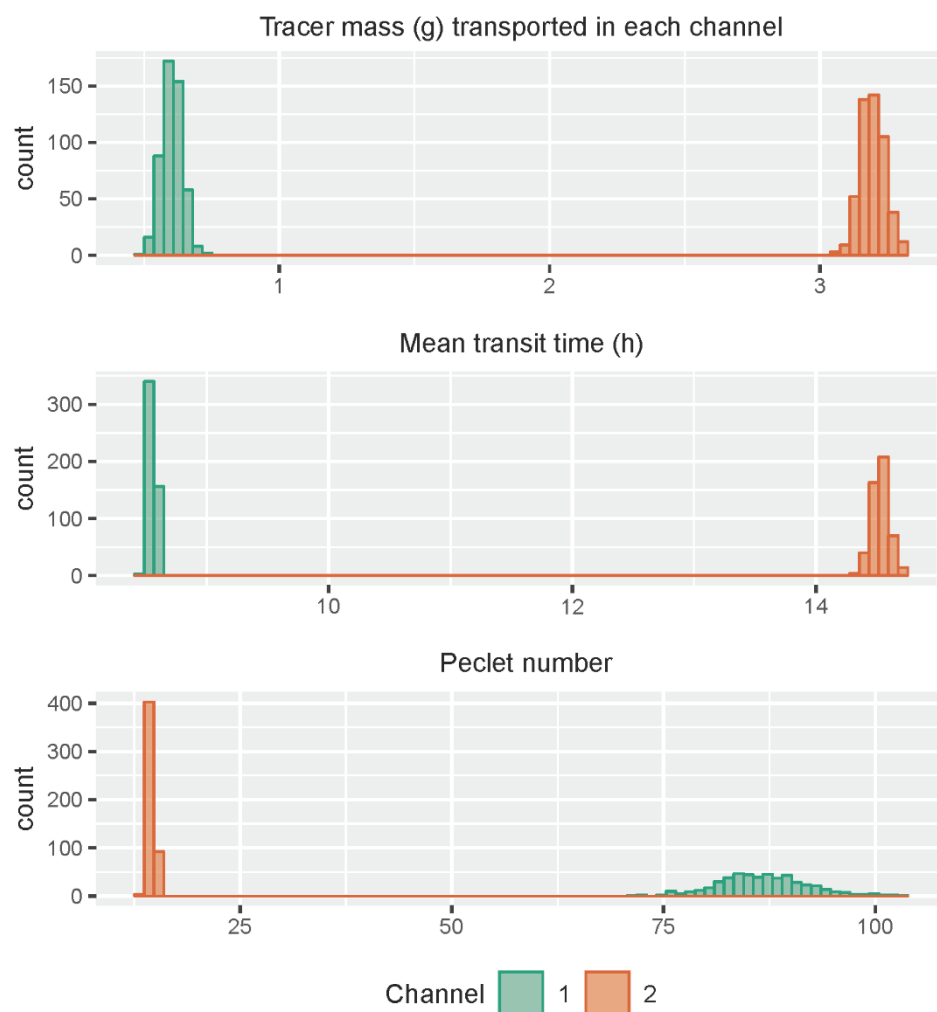
of the M16-M22 tracer BTC.

Figure 6. Postcalibration uncertainty of model parameter values for the inversion of the M16-M22 tracer BTC by a two-channel MDMi model.

6 Summary and conclusions

Multiple flow path transport is likely the rule rather than the exception in most transport problems in fractured and karst aquifers. The main aim of this paper was to present a new curve-fitting tool for the analytical modeling of BTCs from tracer tests performed in such media. The MFIT software is a free open-source Windows-based GUI that provides access to four multiflow transport models. The multiflow approach assumes that the transport from the injection site to the monitoring point takes place in a number of independent 1-D channels. The channels are not assumed to represent individual fractures or karst conduits but are lumped submodels of the main flow routes used by the tracer through the fractures/karst conduit network. The

multiflow modeling framework allows the simulation of multimodal BTCs, which are frequently observed in fractured and karst aquifers. Two of the MFIT transport models combine the multiflow framework and the double-porosity concept, which is applied at the scale of the individual channels. This modeling approach, which has been named MDP, is believed to be new

415   and versatile for the fitting of BTCs with multiple local peaks and/or extensive backward tailing. The accuracy of the MFIT-computed BTCs was verified against two other well-accepted simulation tools for five synthetic test cases.

An important feature of MFIT is its compatibility and interface with the advanced calibration tools of the PEST suite of programs. Hence, MFIT is the first BTC fitting tool that allows regularized inversion and nonlinear analysis of the postcalibration uncertainty of model parameters. Given the nonlinearity of the MFIT model equations, an original multistart

420   algorithm was implemented to maximize the chances for PEST to converge to the global optimal solution in the parameter space during a BTC fitting procedure. The main drawback of the multistart optimization method is that the processing time can be long (up to a few hours) if a large number of channels is assumed in the model. Time reduction for this method is one of the development perspectives of the MFIT code, as the multistart process is computationally parallelizable. Other development perspectives are the management of more complex injection signals, e.g., described as multiple steps, and the

425   implementation of additional analytical transport models for the simulation of reactive transport processes.

Three tracer test BTCs from the HES in Poitiers, France, were used for illustrating the application of the MFIT software. An analysis of the Pareto curves between the model fitting quality and the number of model calibration parameters suggests that the MDMi and MDP-2RNE models are the most appropriate for the interpretation of HES tracer tests. This preliminary result needs to be refined or confirmed by the analysis of additional HES tracer BTCs.

430   **Code and data availability.** The source codes of the MFIT program suite version 1.0.0 are available from https://doi.org/10.5281/zenodo.3470751 under the terms of the CeCILL Free Software License Agreement v2.1 (https://spdx.org/licenses/CeCILL-2.1.html#licenseText, last accessed: 02 October 2019). An "EXE" installation package compiled with Inno Setup (http://www.jrsoftware.org/isinfo.php, last accessed: 02 October 2019) and a user's guide are provided along with the source codes. The following numerical libraries are required for the compilation of the MFIT suite of

435   codes: Boost (https://www.boost.org/, last accessed: 02 October 2019), GSL-GNU (https://www.gnu.org/software/gsl/, last accessed: 02 October 2019), and Spline (https://github.com/ttk592/spline, last accessed: 02 October 2019). The PEST program package is also required for running MFIT. PEST is distributed by default using the MFIT software installer or can be independently downloaded from http://www.pesthomepage.org/Downloads.php (last accessed: 02 October 2019). The data of the HES tracer experiments processed in section 5 of this study are available from the H+ database

440   (http://hplus.ore.fr/en/poitiers/data-poitiers, last accessed: 02 October 2019) through the registration of a free account.

Geoscientific
Model Development
Discussions

References

Abdelaziz, R., Merkel, B. J., Zambrano-Bigiarini, M. and Nair, S.: Particle swarm optimization for the estimation of surface complexation constants with the geochemical model PHREEQC-3.1.2, Geosci. Model Dev., 12(1), 167–177, doi:https://doi.org/10.5194/gmd-12-167-2019, 2019.

450 Anderson, M. P., Woessner, W. W. and Hunt, R. J.: Applied groundwater modeling: simulation of flow and advective transport, Academic Press., 2015.

Arsenault, R., Poulin, A., Cote, P. and Brissette, F.: Comparison of stochastic optimization algorithms in hydrological model calibration, J. Hydrol. Eng., 19(7), 1374–1384, doi:10.1061/(ASCE)HE.1943-5584.0000938, 2014.

Audouin, O., Bodin, J., Porel, G. and Bourbiaux, B.: Flowpath structure in a limestone aquifer: multi-borehole logging
455 investigations at the hydrogeological experimental site of Poitiers, France, Hydrogeol. J., 16(5), 939–950, doi:10.1007/s10040-008-0275-4, 2008.

Berkowitz, B., Cortis, A., Dentz, M. and Scher, H.: Modeling non-Fickian transport in geological formations as a continuous time random walk, Rev. Geophys., 44(2), RG2003, doi:10.1029/2005RG000178, 2006.

Bertrand, G., Celle-Jeanton, H., Huneau, F., Baillieux, A., Mauri, G., Lavastre, V., Undereiner, G., Girolami, L. and Moquet,
460 J. S.: Contaminant transfer and hydrodispersive parameters in basaltic lava flows: artificial tracer test and implications for long-term management, Open Geosci., 7(1), doi:10.1515/geo-2015-0037, 2015.

Bodin, J., Porel, G. and Delay, F.: Simulation of solute transport in discrete fracture networks using the time domain random walk method, Earth Planet. Sci. Lett., 208(3–4), 297–304, doi:10.1016/S0012-821X(03)00052-9, 2003a.

Bodin, J., Delay, F. and de Marsily, G.: Solute transport in a single fracture with negligible matrix permeability: 2.
465 mathematical formalism, Hydrogeol. J., 11(4), 434–454, doi:10.1007/s10040-003-0269-1, 2003b.

Bodin, J., Ackerer, P., Boisson, A., Bourbiaux, B., Bruel, D., de Dreuzy, J.-R., Delay, F., Porel, G. and Pourpak, H.: Predictive modelling of hydraulic head responses to dipole flow experiments in a fractured/karstified limestone aquifer: Insights from a

21

comparison of five modelling approaches to real-field experiments, J. Hydrol., 454, 82–100, doi:10.1016/j.jhydrol.2012.05.069, 2012.

470 Boon, M., Bijeljic, B. and Krevor, S.: Observations of the impact of rock heterogeneity on solute spreading and mixing, Water Resour. Res., 53(6), 4624–4642, doi:10.1002/2016WR019912, 2017.

Chatelier, M., Ruelleu, S., Bour, O., Porel, G. and Delay, F.: Combined fluid temperature and flow logging for the characterization of hydraulic structure in a fractured karst aquifer, J. Hydrol., 400(3–4), 377–386, 2011.

Coats, K. H. and Smith, B. D.: Dead end pore volume and dispersion in porous media, Soc. Pet. Eng. J., 23, 73–84, 1964.

475 Delay, F., Kaczmaryk, A. and Ackerer, P.: Inversion of interference hydraulic pumping tests in both homogeneous and fractal dual media, Adv. Water Resour., 30(3), 314–334, 2007.

Delay, F., Ackerer, P. and Guadagnini, A.: Theoretical analysis and field evidence of reciprocity gaps during interference pumping tests, Adv. Water Resour., 34(5), 592–606, doi:10.1016/j.advwatres.2011.02.006, 2011.

Dentz, M., Le Borgne, T., Englert, A. and Bijeljic, B.: Mixing, spreading and reaction in heterogeneous media: A brief review,
480 J. Contam. Hydrol., 120–121, 1–17, doi:10.1016/j.jconhyd.2010.05.002, 2011.

Doherty, J.: Calibration and uncertainty analysis for complex environmental models, Watermark Numer. Comput. Brisb. Aust., 2015.

Doherty, J.: PEST, model-independent parameter estimation - User manual part I: PEST, SENSAN and global optimisers, Watermark Numer. Comput. Brisb. Aust., 2019a.

485 Doherty, J.: PEST, model-independent parameter estimation - User manual part II: PEST utility support software, Watermark Numer. Comput. Brisb. Aust., 2019b.

Doherty, J. E., Hunt, R. J. and Tonkin, M. J.: Approaches to highly parameterized inversion: A guide to using PEST for model-parameter and predictive-uncertainty analysis. U.S. Geological Survey Scientific Investigations Report 2010–5211, 71 p., 2010.

490 Duan, Q., Sorooshian, S. and Gupta, V.: Effective and efficient global optimization for conceptual rainfall-runoff models, Water Resour. Res., 28(4), 1015–1031, doi:10.1029/91WR02985, 1992.

Espinet, A. J. and Shoemaker, C. A.: Comparison of optimization algorithms for parameter estimation of multi-phase flow models with application to geological carbon sequestration, Adv. Water Resour., 54, 133–148, doi:10.1016/j.advwatres.2013.01.003, 2013.

495 Field, M. S. and Leij, F. J.: Solute transport in solution conduits exhibiting multi-peaked breakthrough curves, J. Hydrol., 440–441, 26–35, doi:10.1016/j.jhydrol.2012.03.018, 2012.

Field, M. S. and Leij, F. J.: Combined physical and chemical nonequilibrium transport model for solution conduits, J. Contam. Hydrol., 157, 37–46, doi:10.1016/j.jconhyd.2013.11.001, 2014.

Gaudard, A., Schwefel, R., Vinnå, L. R., Schmid, M., Wüest, A. and Bouffard, D.: Optimizing the parameterization of deep
500   mixing and internal seiches in one-dimensional hydrodynamic models: a case study with Simstrat v1.3, Geosci. Model Dev., 10(9), 3411–3423, doi:https://doi.org/10.5194/gmd-10-3411-2017, 2017.

van Genuchten, M. T., Simunek, J., Leij, F. J., Toride, N. and Sejna, M.: Stanmod: Model Use, Calibration, and Validation, Trans. Asabe, 55(4), 1353–1366, 2012.

Gharasoo, M., Wietzke, L. M., Knorr, B., Bakkour, R., Elsner, M. and Stumpp, C.: A robust optimization technique for analysis
505   of multi-tracer experiments, J. Contam. Hydrol., 224, 103481, doi:10.1016/j.jconhyd.2019.04.004, 2019.

Goldscheider, N., Meiman, J., Pronk, M. and Smart, C.: Tracer tests in karst hydrogeology and speleology, Int. J. Speleol., 37(1), 27–40, doi:10.5038/1827-806X.37.1.3, 2008.

Gutierrez, A., Klinka, T., Thiery, D., Buscarlet, E., Binet, S., Jozja, N., Defarge, C., Leclerc, B., Fecamp, C., Ahumada, Y. and Elsass, J.: TRAC, a collaborative computer tool for tracer-test interpretation, in EPJ Web of Conferences (Vol. 50, p.
510   03002), EDP Sciences, 2013.

Guvanasen, V. and Guvanasen, V. M.: An approximate semianalytical solution for tracer injection tests in a confined aquifer with a radially converging flow field and finite volume of tracer and chase fluid, Water Resour. Res., 23(8), 1607–1619, doi:10.1029/WR023i008p01607, 1987.

Hansen, N. and Ostermeier, A.: Completely derandomized self-adaptation in evolution strategies, Evol. Comput., 9(2), 159–
515   195, doi:10.1162/106365601750190398, 2001.

Hunt, R. J., Fienen, M. N. and White, J. T.: Revisiting "An Exercise in Groundwater Model Calibration and Prediction" after 30 years: Insights and New Directions, Groundwater, doi:10.1111/gwat.12907, 2019.

Käss, W.: Evaluation and interpretation of tracing tests, in Tracing technique in geohydrology, Balkema, Rotterdam, Netherlands., pp. 372–379, 1998.

520   Käss, W.: Geohydrologische Markierungstechnik, Borntraeger, Stuttgart, Germany., 2004.

Kreft, A. and Zuber, A.: On the physical meaning of the dispersion equation and its solutions for different initial and boundary conditions, Chem. Eng. Sci., 33, 1471–1480, doi:10.1016/0009-2509(78)85196-3, 1978.

Labat, D. and Mangin, A.: Transfer function approach for artificial tracer test interpretation in karstic systems, J. Hydrol., 529, 866–871, doi:10.1016/j.jhydrol.2015.09.011, 2015.

525   Le Coz, M., Bodin, J. and Renard, P.: On the use of multiple-point statistics to improve groundwater flow modeling in karst aquifers: A case study from the Hydrogeological Experimental Site of Poitiers, France, J. Hydrol., 545, 109–119, doi:10.1016/j.jhydrol.2016.12.010, 2017.

Leibundgut, C., Maloszewski, P. and Külls, C.: Mathematical modelling of experimental data: Artificial tracer experiments in multi-flow systems, in Tracers in hydrology, Wiley-Blackwell, pp. 140–144., 2009.

530   Loefgren, M., Crawford, J. and Elert, M.: Tracer tests - possibilities and limitations. Experience from SKB fieldwork: 1977-2007, Swedish Nuclear Fuel and Waste Management Co. [online] Available from: http://inis.iaea.org/Search/search.aspx?orig_q=RN:39028075 (Accessed 2 October 2019), 2007.

Long, A. J.: RRAWFLOW: Rainfall-Response Aquifer and Watershed Flow Model (v1.15), Geosci. Model Dev., 8(3), 865–880, doi:https://doi.org/10.5194/gmd-8-865-2015, 2015.

535   Maloszewski, P. and Zuber, A.: Mathematical modeling of tracer behaviour in short-term experiments in fissured rocks, Water Resour. Res., 26(7), 1517–1528, 1990.

Maloszewski, P., Harum, T. and Benischke, R.: Mathematical modelling of tracer experiments in the karst of Lurbach system, Steirische Beitraege Zur Hydrogeol., 43, 116–136, 1992.

Marino, M. A.: Distribution of contaminants in porous media flow, Water Resour. Res., 10(5), 1013–1018,
540   doi:10.1029/WR010i005p01013, 1974.

Massei, N., Wang, H. Q., Field, M. S., Dupont, J. P., Bakalowicz, M. and Rodet, J.: Interpreting tracer breakthrough tailing in a conduit-dominated karstic aquifer, Hydrogeol. J., 14(6), 849–858, doi:10.1007/s10040-005-0010-3, 2006.

Moreno, L. and Tsang, C. F.: Multiple-peak response to tracer injection tests in single fractures: a numerical study, Water Resour. Res., 27(8), 2143–2150, doi:10.1029/91WR00507, 1991.

545   Neuman, S. P. and Tartakovsky, D. M.: Perspective on theories of non-Fickian transport in heterogeneous media, Adv. Water Resour., 32(5), 670–680, doi:10.1016/j.advwatres.2008.08.005, 2009.

Parker, J. and van Genuchten, M. T.: Determining transport parameters from laboratory and field tracer experiments, Va. Agric. Exp. Stn. Bull., (84–3), 1–96, 1984.

Piotrowski, A. P. and Napiorkowski, J. J.: Optimizing neural networks for river flow forecasting - Evolutionary Computation
550   methods versus the Levenberg-Marquardt approach, J. Hydrol., 407(1–4), 12–27, doi:10.1016/j.jhydrol.2011.06.019, 2011.

Riva, M., Guadagnini, A., Bodin, J. and Delay, F.: Characterization of the Hydrogeological Experimental Site of Poitiers (France) by stochastic well testing analysis, J. Hydrol., 369(1–2), 154–164, doi:10.1016/j.jhydrol.2009.02.040, 2009.

24

Runkel, R. L.: One-dimensional transport with inflow and storage (OTIS): a solute transport model for streams and rivers, U.S. Geological Survey Water-Resources Investigations Report 98-4018, doi:10.3133/wri984018, 1998.

555 Sanchez-Vila, X., Ackerer, P., Delay, F. and Guadagnini, A.: Characterization of reciprocity gaps from interference tests in fractured media through a dual porosity model, Water Resour. Res., 52(3), 1696–1704, doi:10.1002/2015WR018171, 2016.

Sauty, J. P., Kinzelbach, W. and Voss, A.: CATTI: Computer aided tracer test interpretation, BRGM Rep., 1992.

Siirila-Woodburn, E. R., Sanchez-Vila, X. and Fernandez-Garcia, D.: On the formation of multiple local peaks in breakthrough curves, Water Resour. Res., 51(4), 2128–2152, doi:10.1002/2014WR015840, 2015.

560 Singh, S. K., Liang, J. and Bárdossy, A.: Improving the calibration strategy of the physically-based model WaSiM-ETH using critical events, Hydrol. Sci. J., 57(8), 1487–1505, doi:10.1080/02626667.2012.727091, 2012.

Skahill, B. E. and Doherty, J.: Efficient accommodation of local minima in watershed model calibration, J. Hydrol., 329(1), 122–139, doi:10.1016/j.jhydrol.2006.02.005, 2006.

Streetly, H. R., Hamilton, A. C. L., Betts, C., Tellam, J. H. and Herbert, A. W.: Reconnaissance tracer tests in the Triassic
565 sandstone aquifer north of Liverpool, UK, Q. J. Eng. Geol. Hydrogeol., 35(2), 167–178, doi:10.1144/1470-9236/2000-30, 2002.

Tinet, A.-J., Collon, P., Philippe, C., Dewaide, L. and Hallet, V.: OM-MADE: An open-source program to simulate one-dimensional solute transport in multiple exchanging conduits and storage zones, Comput. Geosci., 127, 23–35, doi:10.1016/j.cageo.2019.03.001, 2019.

570 Toride, N., Leij, F. L. and van Genuchten, M. T.: A comprehensive set of analytical solutions for nonequilibrium solute transport with first-order decay and zero-order production, Water Resour. Res., 29(7), 2167–2182, 1993.

Toride, N., Leij, F. J. and Van Genuchten, M. Th.: The CXTFIT code for estimating transport parameters from laboratory or field tracer experiments, version 2.1, Res. Rep. No 137 U Salin. Lab. USDA ARS Riverside CA, 1999.

Tsang, C. F. and Neretnieks, I.: Flow channeling in heterogeneous fractured rocks, Rev. Geophys., 36(2), 275–298, 1998.

575 Wang, J., Wang, C., Rao, V., Orr, A., Yan, E. and Kotamarthi, R.: A parallel workflow implementation for PEST version 13.6 in high-performance computing for WRF-Hydro version 5.0: a case study over the midwestern United States, Geosci. Model Dev., 12(8), 3523–3539, doi:https://doi.org/10.5194/gmd-12-3523-2019, 2019.

Woodward, S. J. R., Wöhling, T. and Stenger, R.: Uncertainty in the modelling of spatial and temporal patterns of shallow groundwater flow paths: The role of geological and hydrological site information, J. Hydrol., 534, 680–694,
580 doi:10.1016/j.jhydrol.2016.01.045, 2016.

Worthington, S. R. H. and Ford, D. C.: Self-organized permeability in carbonate aquifers, Ground Water, 47(3), 326–336, doi:10.1111/j.1745-6584.2009.00551.x, 2009.

Yang, P., Li, Y., Groves, C. and Hong, A.: Coupled hydrogeochemical evaluation of a vulnerable karst aquifer impacted by septic effluent in a protected natural area, Sci. Total Environ., 658, 1475–1484, doi:10.1016/j.scitotenv.2018.12.172, 2019.

585 Zhang, Y., Benson, D. A. and Reeves, D. M.: Time and space nonlocalities underlying fractional-derivative models: Distinction and literature review of field applications, Adv. Water Resour., 32(4), 561–581, doi:10.1016/j.advwatres.2009.01.008, 2009.

Zuber, A.: Theoretical possibilities of the two-well pulse method, Isot. Tech. Groundw. Hydrol. Vol II IAEA, 277–294, 1974.